TANDEM-X SUPPORTED VERTICAL REFLECTIVITY PROFILE CHANGE MONITORING FOR P-BAND

Roman Guliaev, Matteo Pardini, Konstantinos P. Papathanassiou

German Aerospace Center (DLR), Microwave and Radar Institute (HR), Wessling (Germany)

ABSTRACT

Future Synthetic Aperture Radar (SAR) missions, such as ESA'S BIOMASS, will gather vertical reflectivity profiles (VRP) through groundbreaking spaceborne tomographic SAR (TomoSAR) datasets. Monitoring the temporal variations of VRPs on a large scale remains challenging primarily due to insufficient data at a given frequency with an adequate temporal and suitable spatial baseline setups. This challenge has led to the exploration of algorithms capable of approximating VRPs with limited interferometric baselines, such as Polarisation Coherence Tomography (PCT). To expand the observation space, this paper suggests combining data from different frequencies and utilizing multifrequency algorithms. For the first demonstration, X-band interferometric data from TanDEM-X are employed to generate single-baseline PCT VRPs. These PCT VRPs bridge the temporal gap between two airborne tomographic acquisitions in P-band, conducted in 2016 and 2023, as part of the AFRISAR and GABONX campaigns. Additionally, this paper aims to establish a common basis for monitoring changes in VRPs produced by PCT.

Index Terms— InSAR, TomoSAR, Vertical Reflectivity Profile, Polarisation Coherence Tomography

1. INTRODUCTION

TomoSAR techniques are especially useful for mapping forested regions, due to semitransparent microwave nature, revealing structural properties crucial for forest monitoring. Recent years have seen significant advancements in linking TomoSAR vertical reflectivity reconstruction to the actual physical characteristics of forest stands [1] [2].

It is more challenging to examine changes in VRP between acquisitions, especially at global scale due to the scarcity of tomographic data. The primary obstacle in obtaining global tomographic data lies in temporal decorrelation between SAR acquisitions, attributed to changes in dielectric properties and/or wind-induced decorrelations. For example, the selection of P-band for the future BIOMASS mission, coupled with revisit times in the order of a few days, allows to mitigate the temporal decorrelation effect [3].

PCT was proposed as an alternative approach for the reconstruction of VRP from a small set of, or even a single, interferometric coherence measurement [4]. PCT approximates the forest's vertical reflectivity by means of a set of basis functions assuming prior knowledge of forest height and ground terrain elevation. The individual coefficients are estimated from the interferometric coherence measurements.

Methods that can incorporate multi-modal and multifrequency combinations are essential for improving VRP change monitoring. In the following, two techniques, TomoSAR and PCT, and their mutual application at different frequencies and SAR sensor configurations are discussed.

1.1. Tomographic reconstruction of vertical reflectivity profiles

TomoSAR estimates the profile of the backscattered vertical power profiles (VPP) $P(z, \vec{w})$ as a function of the height z and polarization $\vec{w}$. It relies on a set of single-look complex (SLC) SAR images $s_1(\vec{w}), s_2(\vec{w}), \dots, s_M(\vec{w})$ acquired along spatially (and temporal) displaced tracks. The set of the M co-registered and (phase) calibrated SLC images forms the so-called tomographic (data) stack and can be written in form of a (column) data vector $\vec{y}(\vec{w}) = [s_1(\vec{w}), s_2(\vec{w}), \dots, s_M(\vec{w})]^T$ [1] with (M×M)-dimensional covariance matrix:

$$[R] := < \vec{y}(\vec{w}) \cdot \vec{y}^H(\vec{w}) > \quad (1)$$

with $R_{mn} = < s_m(\vec{w})\, s_n^*(\vec{w}) >$. Each element R_{mn} of [R] corresponds to an image pair formed by the m-th and n-th image of the stack and can be related to the VRP $F(z, \vec{w})$ via a Fourier relation:

$$R_{mn} = \int F(z, \vec{w})\, e^{jk_z^{mn} z}\, dz \quad (2)$$

where k_z^{mn} is the vertical wavenumber associated to the pair formed by the m-th and the n-th images of the stack, which is directly proportional to the look angle difference $\Delta\theta$ between the two acquisitions corresponding to their across track separation and inverse proportional to the sine of the incidence angle θ_0.:

$$k_z^{mn} := \frac{2\pi}{\lambda}\frac{\Delta\theta^{mn}}{\sin(\theta_0)} \quad (3)$$

The VPP can be reconstructed from covariance matrix [5]

$$P(z) = \vec{h}(z)^H [R] \vec{h}(z) \quad (4)$$

The generic filter $\vec{h}(z)$ is designed to allow only the backscatter contribution at z_i to pass, while cancelling out the contributions at the other heights. In the following, the Fourier beamforming filter will be used.

1.2. Polarisation Coherence Tomography

Interferometric SAR measurements are inherently dependent on the vertical structure of volume scatterers as forests are. The complex, polarization dependent, interferometric coherence between two interferometric SAR images at a given polarization $\vec{w}$, $s_1(\vec{w})$ and $s_2(\vec{w})$, acquired by an the across track separation (e.g. baseline) is defined by their normalized statistical product as [6]

$$\tilde{\gamma}_{Obs}(\vec{w}) = \frac{< s_1(\vec{w}) s_2^*(\vec{w}) >}{\sqrt{< s_1(\vec{w}) s_1^*(\vec{w}) >< s_2(\vec{w}) s_2^*(\vec{w}) >}} \quad (5)$$

Symbol <⋯> represents the statistical expectation, and it is typically estimated through the averaging of adjacent samples within a range-azimuth (multilook) cell, assuming ergodicity.

The measured interferometric coherence can be written as the product of independent decorrelation contributions, including temporal decorrelation $\tilde{\gamma}_{Tmp}(\vec{w})$ and various system-induced decorrelations such as additive noise decorrelation $\tilde{\gamma}_{Sys}(\vec{w})$ [6] [7]

$$\tilde{\gamma}_{Obs}(\vec{w}) = \tilde{\gamma}_{Tmp}(\vec{w})\tilde{\gamma}_{Rg}(\vec{w})\tilde{\gamma}_{Sys}(\vec{w})\tilde{\gamma}_{Vol}(\vec{w}) \quad (6)$$

The coherence contribution that reflects the vertical structural properties of the scattering volume is the volumetric decorrelation, which can be written [8]

$$\tilde{\gamma}_{Vol}(\kappa_z, \vec{w}) = e^{j\phi_0}\frac{\int_0^1 F(z', \vec{w})\, e^{jk_z h_v z'} dz'}{\int_0^1 F(z', \vec{w})\, dz'} \quad (7)$$

The phase term ϕ_0 corresponds to the height of the underlying terrain and h_V is the vertical size of the reflectivity volume, i.e. in forests it is the forest height.

Equation (7) contains the information about both the extent of the volume, i.e. forest, as well as its (vertical) structural properties (vertical reflectivity function) [9].

Assuming forest height and ground phase to be known, it is possible to formulate the estimation of $F(z, \vec{w})$ from (7) by means of a linear system of equations. For this $F(z, \vec{w})$ is expanded in terms of a set of N basis functions $f_0(z), .., f_N(z)$ with corresponding (real valued) coefficients $a_1, .., a_N$

$$F(z, \vec{w}) \approx a_0(\vec{w})f_0(z) + a_1(\vec{w})f_1(z) + \cdots + a_n(\vec{w})f_N(z) \quad (8)$$

Depending on the number M of available interferometric acquisitions (each providing a single $\tilde{\gamma}_{Vol}^m(\kappa_z, \vec{w})$) with vertical wavenumber k_z^m a maximum number of N=2M coefficients a_n can be estimated. Accordingly, for the single-baseline case, i.e. M=1, the reflectivity function is approximated by N=2 coefficients as $F(z, \vec{w}) \approx a_0(\vec{w})f_0(z) + a_1(\vec{w})f_1(z) + a_2(\vec{w})f_2(z)$ so that (7) after compensation of ϕ_0 can be rewritten as

$$\tilde{\gamma}_{Vol}^m(\kappa_z, \vec{w}) = \frac{\int_0^1 [a_0(\vec{w})f_0(z) + a_1(\vec{w})f_1(z) + a_2(\vec{w})f_2(z)]\, e^{jk_z^m h_v z} dz}{\int_0^1 [a_0(\vec{w})f_0(z) + a_1(\vec{w})f_1(z) + a_2(\vec{w})f_2(z)]\, dz} \quad (9)$$

Solving two linear equations, associated to the real and imaginary part of (9), enables the determination of a_1 and a_2, which is referred to the Polarisation Coherence Tomography (PCT) method [4]. Note that the normalization in (7) cancels out the zeroth order coefficient a_0. Consequently, it allows the estimation of a relative vertical reflectivity. The reconstruction of $F(z, \vec{w})$ is performed for every polarization $\vec{w}$ independently. Since this work is concerned only with the reconstruction of $F(z, \vec{w})$ at a single polarisation, the polarisation dependence is suppressed in the following.

The choice of basis functions affects $f_0(z), .., f_N(z)$ the reconstruction of the VRP. Originally the Legendre series were implemented [4]. This paper proposes the use of data-driven basis types [9].

2. DEMONSTRATION ON REAL DATA

The fully polarimetric tomographic data, used in the following, were acquired by DLR's F-SAR airborne sensor over the Mondah rainforest site in Gabon in the frame of the AfriSAR in February 2016 and GABONX in May 2023 campaigns [10] [11]. Fig. 1 shows the Pauli images of both missions, where white line refers to the extracted tomographic slice, analysed in the following.

Fig. 1 Pauli images of P-band F-SAR acquisitions from AfriSAR campaign in 2016 and GABONX in 2023. The tomographic profiles were extracted along the white line.

Interferometric X-band data (9.8 GHz) with 100 MHz bandwidth data were acquired by TanDEM-X in a stripmap HH-polarization mode with an average incidence angle of 40º. The acquisitions over the Mondah site were performed between 2015 and 2019 with vertical wavenumbers varying from 0.06 to 0.13 rad/m corresponding to ambiguity heights of 50 to 140 meters (see Table 1) along descending orbits. The TanDEM-X Coregistered Slant Range Single Look Complex (Co-SSC) data have been 10 x 10 multi-looked in pixels along range and azimuth to produce complex interferometric coherence data and georeferenced in latitude / longitude coordinates to an approximate grid size of 20m x 20m. The volumetric decorrelation was calculated from interferometric coherence after compensating for additive noise decorrelation, whereas temporal decorrelation and various system induced decorrelations were assumed to be negligible.

Date	k_z [rad/m]	Ambiguity Height [m]	Orbit
11/11/2015	0.062	101.3	Desc
17/11/2017	0.123	51.1	Desc
04/07/2019	0.123	51.1	Desc

Table 1 TanDEM-X acquisition parameters.

The tomographic VPPs from P-band at HV-pol channel along the white line in Fig. 1, are presented in Fig. 2 for the AfriSAR mission in 2016 (top row) and GABONX mission in 2023 (bottom row). The 10 tomographic baselines were acquired in the same configuration for both missions.

To bridge the two tomographic observations, the PCT estimated VRPs at X-band were produced using TanDEM-X bistatic InSAR acqusitions with Legendre basis. These VRPs are shown in 2nd to 4th row of Fig. 2 for acquisition years of 2015, 2017 and 2019.
The underlying ground height z_0 and the associated phase ϕ_0 was then estimated from the lowest peak in the ground-only VPP P (z) within the interval of $z_{DEM} - 50m < z < z_{DEM} + 30m$ as described in [12], [13].

The upper boundary was estimated from the volume-only vertical power profiles from the position of 3dB attenuation of the highest peak within the interval of $z_{DEM} - 50m < z < z_{DEM} + 30m$.

Next, the P-band basis basis was produced, using the method outlined in [9]. Fig. 3 demonstrates the PCT VRPs reconstructed using the P-band basis across both P-band and X-band interferometric data. This allows to compare and monitor changes at VRPs produced by the same PCT method with one frequency derived basis.

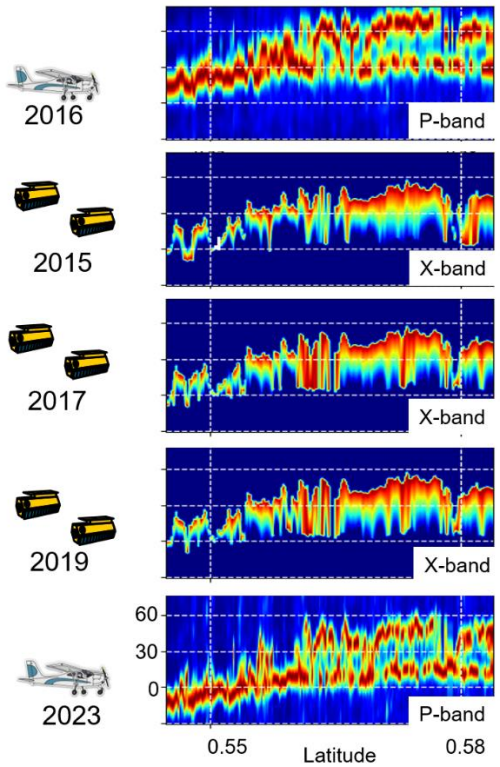

Fig. 2 VRP reconstructions from top to bottom: F-SAR P-band HV-pol Fourier Beamforming in 2016, TanDEM-X PCT with Legendre basis in 2015, 2017, 2019; F-SAR P-band HV-pol Fourier Beamforming in 2023

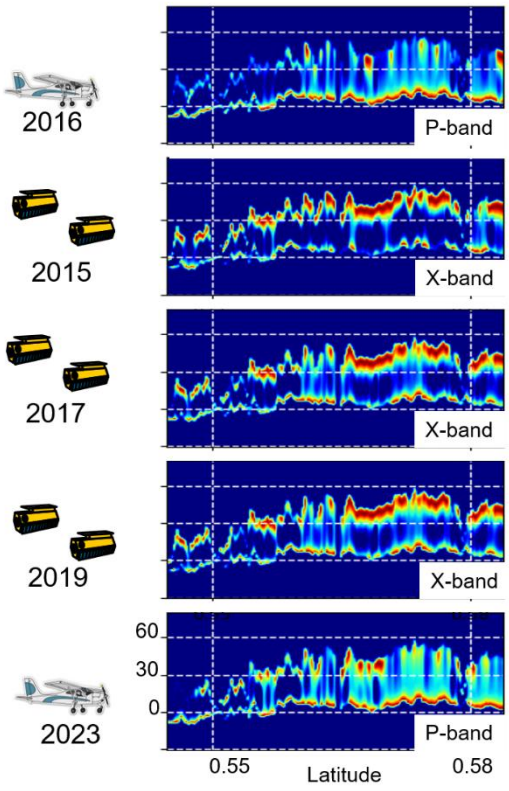

Fig. 3 VRP reconstructions from top to bottom: F-SAR P-band HV-pol PCT with P-band basis in 2016, TanDEM-X PCT with P-band basis in 2015, 2017, 2019; F-SAR P-band HV-pol PCT with P-band basis in 2023

2. OUTLOOK

The use of interferometric data and the PCT method enables the production of single-baseline VRPs, effectively bridging the temporal gap between tomographic acquisitions. TanDEM-X provides bistatic interferometric data, facilitating the reconstruction of single-baseline PCT VRPs. With the continued operation of TanDEM-X, there is potential for it to serve in monitoring VRP changes as measured by BIOMASS. Given the increasing number of missions operating at different frequencies and interferometric setups, a holistic approach becomes essential. Future research will aim at multifrequency and multimodal approach, crucial for facilitating change monitoring in rainforests.

4. REFERENCES

[1] A. Reigber and A. Moreira, " First demonstration of air-borne SAR tomography using multibaseline L-band data," *IEEE Trans. Geosci. Remote Sens.*, vol. 38, no. 5, pp. 2142-2152, Sept. 2000.

[2] V. Cazcarra-Bes, M. Tello-Alonso, R. Fischer, M. Heym and K. Papathanassiou, "Monitoring of Forest Structure Dynamics by Means of L-Band SAR Tomography.," *Remote Sens.* , vol. 9, p. 1229, 2017.

[3] S. Quegan, T. Le Toan, J. Chave, J. Dall, J. Exbrayat, D. Minh, M. Lomas, M. D'alessandro, P. Paillou, K. Papathanassiou and F. Rocca, "The European Space Agency BIOMASS mission: Measuring forest above-ground biomass from space," *Remote Sensing of Environment,* no. 227 , pp. 44-60, 2019.

[4] S. Cloude, "Polarization coherence tomography," *Radio Science* , no. 41.04, pp. 1-27, 2006.

[5] F. Lombardini and A. Reigber, "Adaptive spectral estimation for multibaseline SAR tomography with airborne L-band data," in *IGARSS IEEE International Geoscience and Remote Sensing Symposium IEEE Proceedings (IEEE Cat. No. 03CH37477)*, 2003.

[6] G. Krieger, A. Moreira, H. Fiedler, I. Hajnsek, M. Werner, M. Younis and M. Zink, "TanDEM-X: A satellite formation for high-resolution SAR interferometry," *IEEE Transactions on Geoscience and Remote Sensing,* vol. 45, no. 11, pp. 3317-3341, 2007.

[7] G. Krieger, K. P. Papathanassiou and S. R. Cloude, "Spaceborne polarimetric SAR interferometry: performance analysis and mission concepts," *EURASIP J. Applied Sig. Proc. 20,* pp. 3272-3292, 2005.

[8] K. Papathanassiou and S. Cloude, "Single-baseline polarimetric SAR interferometry," *IEEE Trans. Geosci. Remote Sens,* vol. 39, no. 11, pp. 2352-2363, 2001.

[9] R. Guliaev, V. Cazcarra-Bes, M. Pardini and K. Papathanassiou, "Forest Height Estima-tion by Means of TanDEM-X InSAR and Wave-form Lidar Data.," *IEEE Journal of Selected Topics in Applied Earth Observations and Remote Sensing,* vol. 14, pp. 3084-3094, 2021.

[10] I. Hajnsek, M. Pardini, et al.,, "Technical assistance for the development of airborne SAR and geophysical measurements during the AfriSAR campaign, Final technical report".

[11] T. Fatoyinbo et al., "The NASA AfriSAR campaign: Airborne SAR and lidar measurements of tropical forest structure and biomass in support of current and future space missions," vol. 264, p. 112533, 2021.

[12] M. Pardini, M. Tello, V. Cazcarra-Bes, K. Papathanassiou and I. Hajnsek, "L-and P-band 3-D SAR reflectivity profiles versus lidar waveforms: The AfriSAR case.," *IEEE Journal of Selected Topics in Applied Earth Observations and Remote Sensing,* vol. 1, 2018.

[13] M. Pardini, V. Cazcarra-Bes and K. P. Papathanassiou, "TomoSAR Mapping of 3D Forest

Structure: Contributions of L-Band Configurations,"
Remote Sensing, vol. 13, no. 12, p. 2255, 2021.